Original Research Paper

IJES *Iranian Journal of Earth Sciences*
Vol. 14, No. 3, 2022, 165-177.
DOI: 10.30495/ IJES.2022.1947113.1690

Near surface cavities mapping using integrated geophysical techniques: Case study of Gadwalian dam, North Pakistan

Waqar Ahmad[*1,2], Khaista Rehman[2], Muhammad Farooq[3], Asghar Ali [4], Tanveer Ahmed[2]

1. School of Geography and Ocean Science, Nanjing University, Nanjing 210023, PR China
2. National Centre of Excellence in Geology, University of Peshawar, Khyber Pakhtunkhwa 25130, Pakistan
3. Department of Geology, University of Azad and Jammu Kashmir, Pakistan
4. Department of Geology, University of Peshawar, Khyber Pakhtunkhwa 25120, Pakistan

Received 23 December 2021; accepted 3 March 2022

Abstract

Integrated geophysical techniques have always been useful in identifying subsurface features. In the present study, three integrated geophysical methods of ground-penetrating radar (GPR), resistivity and Multi-channel Analysis (MASW) of surface waves have been utilized for near surface studies and identification of subsurface cavities near the Gadwalian dam. Acquisition of four inline and crossline profiles through GPR (100 MHz shielded antenna), two resistivity profiles through Imaging system and six seismic refraction profiles (MASW) have been made on the selected site having potential subsurface cavities. The processing and interpretation of GPR data through different software's exhibit variations in amplitude/diffraction patterns and several cavities have been identified in the GPR profiles. Sweetness attributes applied on the GPR data set also validate the cavities and unsaturated/saturated fractures. Slate beds and cavities have also been identified on pseudosections obtained through resistivity imaging. Further studies on 2D shear velocity (Vs30) profiles using MASW analysis for interpretation suggested that the absence of low velocity layer in shallow surface and velocity increase with respect to depth.

Keywords: *GPR, ERT, MASW, near-surface cavities, pseudosection, dam studies.*

1. Introduction

Dams are constructed for electricity generation, irrigation purposes, flood control, and recreation purposes. Seepage, internal erosion, and after overtopping at high flooding discharge causes dam failures in most cases. Examples of dam failure related to seepage are Malpaset dam failure and Teton dam failure (Seed and Duncan 1981; Cedergren 1997). Malpaset dam failure occurred because of excessive pressure of water in rock seams and failure of Teton dam happened by seepage of water in joint cracks inside the foundation of the dam. The study area is situated in Gandghar Range near Gadwalian dam, District Haripur (Fig 1). In the south-east direction the Gandghar range bounded by Margala Hills and in the east by Khanpur Hills (Yeats and Hussain 1987).

In this area the Panjal fault constituting Hazara Kashmir syntaxis recognized by Wadia (1957) and along this fault the Gandghar range has been uplifted. A suite of meta sedimentary rocks exposed in the Gandghar range which have been correlated with the Palaeozoic sequence of Hazara and the Attock-Cherat Range (Tahirkheli 1971). pegmatites, hydrothermal and metasomatic rocks, as well as in many ore deposit types. Some of the karstic features have been observed on the surface in the study site during the reconnaissance survey and these karstic features can be hazardous to the dam main reservoir (Fig 2). For evaluation of dam sites and highways, non-destructive, cost and time-effective geophysical techniques have been widely used from the last few decades. Commonly used geophysical techniques for evaluation purposes by researchers are electrical resistivity, seismic surface waves, Ground Penetrating Radar (GPR), seismic reflection method (Cook 1965; Smith 1986; Steeples and Miller 1987; Chamberlain et al. 2000; Gibson et al.2004; Thierry et al. 2005; Ismail and Anderson 2007; Mochales et al. 2008; Gambetta et al. 2011; Loke 2012; Nouioua et al. 2013; Azeem et al. 2021). In general, these methods have been widely used for near-surface investigation, lateral and vertical changes in soil properties, bed-rock identification, caves/cavities detection and groundwater table depth identification. In this study, we have conducted different types of geophysical data for the identification of subsurface cavities and the characterization of the near-surface left bank of the main reservoir of the Gadwalian dam. The pathway to the western side of the dam has been utilized for acquisition that was originally built for the transportation of heavy vehicles and having the concerned formation exposure of up to 100 m. For evaluation purposes inside the pathway upper layer of hard bedrock have been identified with potential sinkholes, voids, dissolutions, or subsurface lateral variations that can lead to instability in the main bank of the dam. Three geophysical techniques have been utilized in this study including GPR, MASW and Electrical Resistivity Tomography (ERT) to investigate the subsurface adjacent bank of the Gadwalian dam.

---

*Corresponding author.
E-mail address (es): waqarjadoon@uop.edu.pk

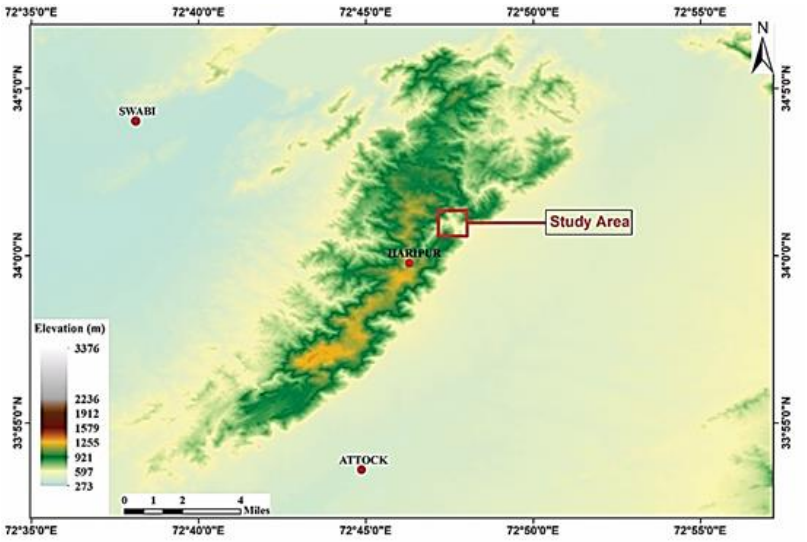

Fig 1. Regional Map of the area under investigation

Fig 2. Karstic features observed on the surface near dam site. (a) Cavity formed due to dissolution of limestone (b) Limestone dissolution developing cavities and cracks (c) GPR data acquisition in the study area and (d) Gadwalian Dam main reservoir view

Reflection amplitude and transmitted velocity of electromagnetic waves data has been acquired through GPR which depicted cavities or sinkholes, subsurface voids, vertical and lateral variations in soil type, groundwater table depth. 1D and 2D profiles of subsurface have been generated by data acquisition of shear wave velocity through the MASW method. The S-wave velocity indicates the strength of soil, bedrock mapping, and stiffness of soil. Through ERT, the variations in soil moisture contents, porosity, and clay contents have been observed on the basis of their electrical behavior (Reynolds 2011). Three geophysical techniques results have been illustrated for characterization and identification of potential hazards along with the dam site.

Several geophysical studies have been carried out in the past for detection of cracks, fractures and fissures causing seepages that are considered hazardous for mega

structure constructions (e.g. Butler and Llopis 1990; Sjödahl et al. 2009; Xu et al. 2010; Farooq et al. 2012; Chinedu and Ogah 2013; Ilesanmi et al. 2013; Moreno 2015; Alemaw et al. 2016; Jehangir Khan et al. 2021). Gadwalian dam is a newly constructed dam and till date no feasibility study or survey has been conducted for prevention of such karstic features. Furthermore, no published work has been reported on cavities detection in such type of areas. There are also some limitations of each geophysical method for exploration purposes. Therefore, an integrated approach comprising of different geophysical techniques has been adopted for comparative analysis, checking the reliability of each method and investigation of subsurface cavities for previously unexplored area.

2. Geology of the study area

Geological investigation show that the bedrock of study site belongs to southeastern part of Northern Gandghar range. According to Hylland et al. (1988) and Riaz et al. (1991) The northern Gandghar Range consists of four stratigraphic successions (Table 1). Manki Formation composed of slates and phyllites forming the basal sequence, two carbonate lithologies (Shahkot and Shekhai Formations) overlain the basal sequence and an alternating sequence (Tanawal Formation) composed of quartzite and phyllite. Basic igneous dikes and sills of unknown age intruded abundantly in the entire succession. Baghdarra fault separated the Northern Gandghar range into a western and an eastern structural block.

Shekhai formation is exposed in the study site having massive limestone forming the footwall of Baghdarra fault (Hylland 1990; Riaz et al. 1991). Detailed Geological mapping by Hylland (1990) shown that this formation composed of marble and limestone with subordinate shale, quartzite and argillite. Occasionally massive unit of limestone is thin to medium bedded and fined grained. The limestone is light gray and yellowish gray but light brown and brownish gray or pink beds are also seen. Near igneous intrusions, the limestone is locally metamorphosed to creamy or white marble. Shale and argillite are mostly greenish-gray, green, occasionally calcareous and thinly laminated at some places (Tahirkheli 1971; Hylland 1990; Riaz et al. 1991).

Table 1 Stratigraphy of Northern Gandghar Range with formation names, age and lithological Description (Riaz et al. 1991).

Age	Formation	Members	Description
Early to Middle Cambrian	Tanawal Formation	Basal conglomerate member	Quartzite and sandstone
		Middle quartzite member	Quartzites and phyllites
		Upper quartzite member	Quartzite with shaley partings
Late Precambrian	Shekhai Formation		Limestone, marble, argillite, shale and quartzite
Precambrian	Shahkot Formation		Limestone, argillite and shale
Precambrian	Manki Formation		Argillites, slates, phyllites and minor limestone

3. Methodology

The location of the selected site was the left bank of the Gadwalian dam near District Haripur (Fig 1). The dam was originally constructed for irrigation purposes in late 2017. With the passage of time, the dam site has been affected by landslides and dissolutions which are also visible on surface.

Similar dissolutions phenomena might have been occurred in subsurface resulted in voids, cavities, and sinkholes. To observe this phenomenon in the subsurface and investigating the potential hazards for dam life, the site has been evaluated through integrated geophysical data acquisitions. The present work utilizes Ground Penetrating Radar (GPR), ERT and MASW in the selected site for identification of potential hazards. Data acquisition for each geophysical technique has been made along profile lines. The following mechanism has been adopted for each geophysical technique. GPR is used to measure the electromagnetic discontinuities in the subsurface and the measurement is in the form of dielectric constant of the transmitted signal. The GPR data acquisition diagram and instrument are shown in Figs. 3 and 4 respectively.

GPR consists of mainly four parts: 1) transmitting antenna; 2) receiving antenna; 3) monitor; and 4) control unit (Xu et al., 2010). Pulling technique of GPR antenna is applied over the site of investigation and subsurface variations are measured in the form anomalies.

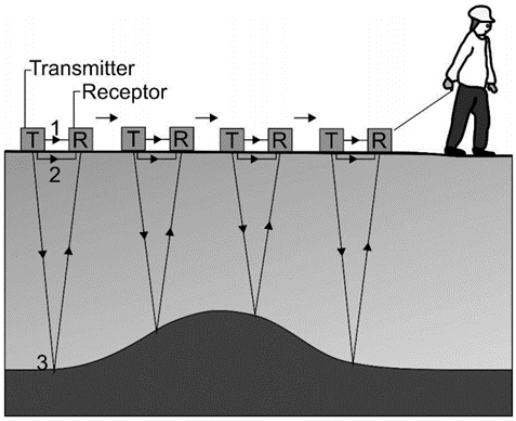

Fig 3. Basic principle of GPR instrument (Moreno, 2015).

High frequency antenna gives shallow depth and vice versa. Similarly, low frequency antenna provides deeper targets anomalies with low resolution. More detailed discussion about acquisition, processing and interpretation techniques can be found in Robinson and Çoruh (1988) and Reynolds (2011), and their approach is applied here.

The following equation is used for electromagnetic wave velocity of subsurface material (Flohrer and Pöpel 1996):

$$v = C/\sqrt{\varepsilon\gamma} \quad (1)$$

where C is the speed of light and $\varepsilon\gamma$ represent dielectric constant.

Similarly, following equation is used for distance among antennas.

$$d = \frac{v.\Delta T}{2}v \quad (2)$$

velocity, v can be estimated from equation (1) and ΔT refers to the time from emitting to receiving antenna.

Reflecting coefficient (r) can be calculated by using following equation:

$$r = \frac{1-\sqrt{\varepsilon_2/\varepsilon_1}}{1+\sqrt{\varepsilon_2/\varepsilon_1}} \quad (3)$$

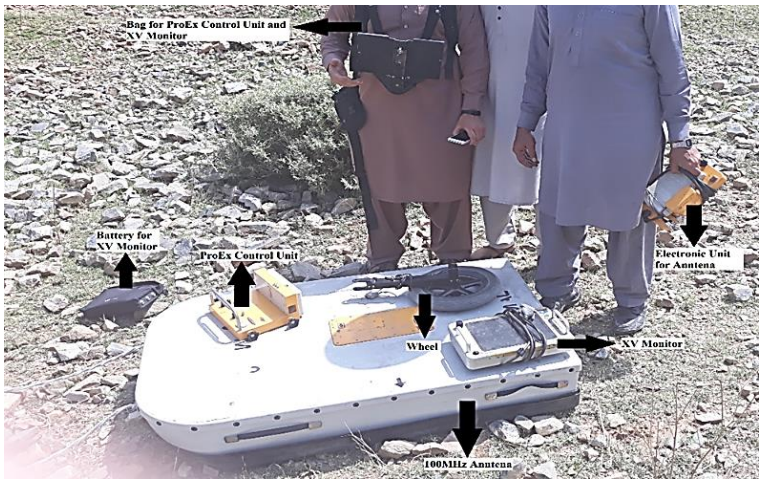

Fig 4. Complete GPR Survey Instrument used for acquiring the data.

For cavities and other features identification, sweetness attribute has been applied which is based on the reflection strength of subsurface lithologies, envelop attribute and instantaneous frequency attribute. Strong reflections are found in karst as well as in carbonates cavities. According to Hart (2008), clay filled cavities (water) absorb high frequency signals of radar. In case of GPR acquisition for current studies, four profile lines have been taken comprising of three (3) in-lines and one cross lines in accordance with surface geology and topography of the study area (Fig 5). Similarly, for sweetness attribute analysis, after merging SEG-Y and navigation files, in Petrel platform, profile 1 and 2 have been analyzed intensely for illustration.

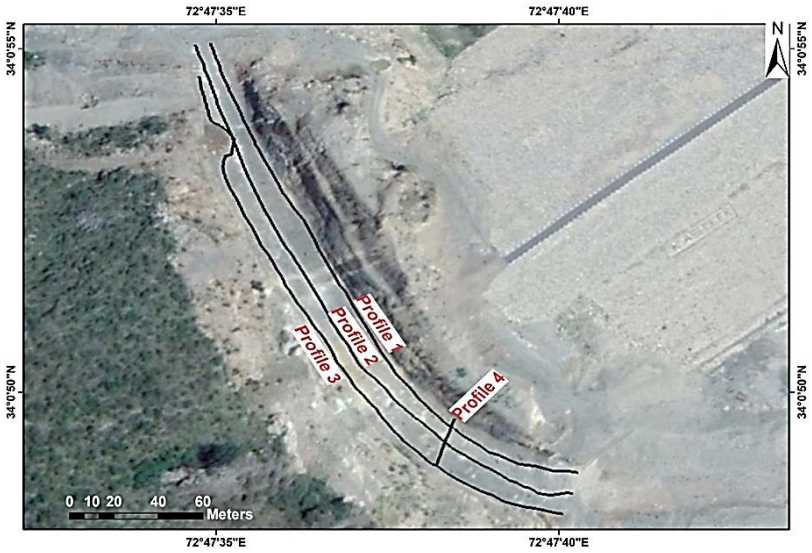

Fig 5. Plan showing location of GPR profiles (1−4)

The shear wave velocity (V_s) for subsurface low velocity layer using MASW is the measurement parameter used in seismic refraction method. Geode instrument is used to measure the V_s values at each observation point on the surface. The fundamental mode of Rayleigh waves utilize the dispersive properties of surface waves while these are considered to be noise in reflection method (Park et al. 1999). The particle motion of Rayleigh waves is shown in Fig 6. This type of Rayleigh waves is also used in geotechnical applications.

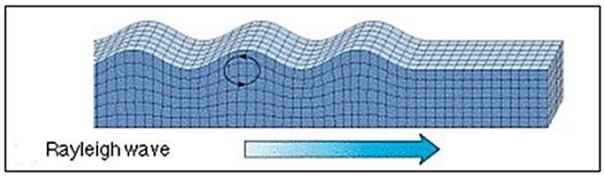

Fig 6. Rayleigh wave diagram showing particles motion.

V_s can be estimated by the following equation:

$$\mu = V_s{}^2 \rho \quad (4)$$

Where (ρ) is the mass density and (μ) is the shear modulus.

$$E = 2\,\mu\,(1+\nu) = V_s{}^2 \rho(1+\nu) \quad (5)$$

ν represents Poisson's ratio and for sands and gravels its value ranging from 0.25 − 0.35 (Bessason and Erlingsson 2011).

By solving equation (5) following equation for V_s is obtained:

$$V_s = \sqrt{\frac{\mu}{\rho}} = \sqrt{\frac{E}{2\rho(1+\nu)}} \quad (6)$$

In the MASW method, six linear traverses have been acquired in the study area including five 5 traverses of 24 m length and one traverse were 12 m using spread geometry of 24 geophones having 14-Hz low-frequency (Fig 7). Spacing interval of the geophones has been kept constant at one meter. A hammer having weight of 10 kg has been used as a source and two meters distance kept between the first geophone and source. Two stacks have been taken at each location using forward shooting only. The sampling periods for all 24 tracks were 0.25 msec and the total acquisition duration was 400 msec. The acquired data of MASW has been further processed and interpreted through software with graphical display. In the first step of MASW analysis by using Fast Fourier Transform (FFT) method the acquired data were converted from the time domain to the frequency domain (Park et al. 1999). In the second step, converted data has been used to extract the dispersion curve (graph between frequency and phase velocity) (Duffy 2008). In the last step, from the dispersion curve, an iterative non-linear inversion process has been used to calculate Vs (Xia et al. 1999). After the inversion process, different physical properties i.e. P-wave velocity (Vp), thickness (H) and density (r) of different sub-surface mediums have been calculated. In general, the parameter of Vs is mostly use for soil classification and micro-zonation (Dobry et al. 2000; Wills 2000; Andrus and Stokoe 2000). For the 2-D profile plot, the data has been transferred to Surfer Software for interpolation by using the Kriging algorithm.

Subsurface resistivity can be calculated by using Ohm's principle and it can be written as:

$$I = \frac{V}{R} \quad \text{or} \quad R = \frac{V}{I} \quad (7)$$

The detailed information about resistivity technique, conventional electrodes of current and potential are described in Robinson (1988).

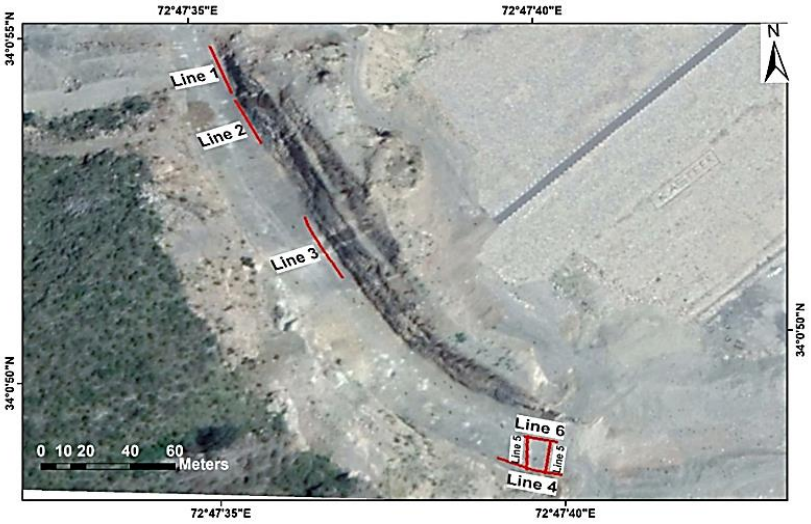

Fig 7. Plan showing location of Geode lines (1–6) that are acquired for MASW

Following equations are used for the current and potential electrodes arrangement:

$$V_M = \frac{1\rho}{2\pi}\left[\frac{1}{AM} - \frac{1}{BM}\right]; \quad V_N = \frac{1\rho}{2\pi}\left[\frac{1}{AN} - \frac{1}{BN}\right] \tag{8}$$

Where (V_M) and (V_N) refers to potential and current electrodes arrangement respectively, A

Where (VM) and (VN) refers to potential and current electrodes arrangement respectively, A and B represents current electrodes and M and N shows potential electrodes.

Equation (9) represents the potential difference between current electrodes:

$$\Delta V_{MN} = \frac{1\rho}{2\pi}\left[\frac{1}{AM} - \frac{1}{BM} - \frac{1}{AN} + \frac{1}{BN}\right] \tag{9}$$

The apparent resistivity is given by:

$$\rho_a = R.K \tag{10}$$

Where ρ_a represents apparent resistivity (Ω-m). R= ΔV/I. K is called geometric factor.

K is calculated using following equation:

$$K = \frac{2\pi}{\left[\frac{1}{AM} - \frac{1}{BM} - \frac{1}{AN} + \frac{1}{BN}\right]} \tag{11}$$

In case of homogeneous and shallow targets, the real and apparent resistivity values coincide during measurement. We get the apparent resistivity values in during acquisition using Terrameter. After applying the inversion techniques of Jacobian matrix, values of real resistivity can be obtained. An iterative approach is used for real resistivity modeling using best fitting model of apparent resistivity values.

For imaging of subsurface and hazards exploration, electrical resistivity tomography has been used by using the Lund imaging system (Fig 8). ERT having higher resolution provides better results in comparison with other point measurements and soundings. In imaging, both vertical and lateral subsurface variations of resistivity have been observed along the survey line (Thierry et al. 2005; Rybakov et al. 2005; Alastruey et al. 2002).

Fig 8. ERT equipment set-up: A. Main instrument of Terrameter (SAS 4000); B. Electrode selector model (ES10-64C); C. Electrode Cable rolls; D. Steel electrodes for data acquisition; E. Connectors cable-electrode; F. Battery for current supply; G. Cable connecters; H. Terrameter and electrode selector connector and I. Data transferring cable from Terrameter to laptop.

Fig 9. Plan showing location of imaging-based ERT profiles (1 and 2)

Using ERT, resistivity has been acquired along two profile lines ABEM SAS-1000 basic unit with imaging system attached (Fig 9). The ERT profile lines were not linear similar to data acquired through GPR because of poor current penetration pitfall despite of using saline mud with electrodes installation in the study area (Loke 2015).

For that reason, electrodes were mounted in a curvilinear direction at the end of profiles instead of linear alignment. Acquired data has been transferred to Res2d software for further processing. In processing the data has been filtered for signal to noise ratio enhancement and removal of vague data in profiles that can affect the inversion. The least-square method has been utilized in inversion process keeping the RMS error low. Following the set workflow, true resistivities of the subsurface lithologies have been obtained. Transition boundaries have been defined through this method that can be difficult to determine through other geophysical techniques.

4.Results and Discussions

In this study, five analyses, (1) Generation of final results of GPR radargram (amplitude of reflectors vs. time, depth and distance) (Fig 10 and 11), (2) sweetness attribute from GPR data (Fig 12: un-interpreted cross-section of GPR profile-1; Fig 13: interpreted cross-sections; Fig 14: un-interpreted cross-section of GPR profile-2; Fig 15: interpreted cross-sections), (3) From 1D MASW results, producing 2D model (Shear wave velocity vs. depth and Geophone distance) (Fig 16) (4) 2D models creation of ERT (subsurface resistivity vs. depth and distance), have been used (Fig 17 & 18), and (5) integration and comparison of the results of GPR, MASW, and ERT techniques with limitations have also been described.

GPR data has been acquired along profile lines having different orientations. The total lateral distance and depth of profile-03 having orientation in NW to SE direction is 233 meters (m) and 11.5 m respectively (Fig 10). Profile-4 has the orientation in NE to SE direction is having total lateral distance of 16.5 m and a depth of 10.5 m (Fig 11). These two profiles depict several subsurface cavities detected at a different lateral distance. The profile line 3 show that first cavity has been identified at a distance of 10 meters (m) and a depth of 2.5 m similarly, the second, third, fourth, fifth, and sixth cavity has been identified at 110 m, 145 m, 165 m, 192 m, and 220 m distances respectively. Below the depth of 5 meters in GPR profiles, the resolution of data was low due to which cavities were not visible properly however, the hyperbolas depict the zones of potential cavities (Fig 10). At a distance of 2 m, the first large cavity was detected at a depth of 3.5 m and the other two cavities are shown at a distance of 11 and 14 m having 3 m depth (Fig 11). The interpretation results of these profiles shows that shallow cavities are located at several distances and depth ranges at 3-5 m. Near-surface the strong reflections represent that bedrock is directly exposed and for GPR measurements a direct contact with the bedrock surface has been required. Bushes, cut brush and trees are great obstacles during GPR data acquisition (Łyskowski et al. 2014). It is important to note that the GPR parameters like frequency, depth, resolution, and lithology have mutual dependence, i.e. for better resolution, a high-frequency antenna is used however, it reduces the penetration depth, and vice versa.

For Sweetness attribute analysis, two GPR inlines Profiles 1 and 2 have been used. Profile-1 having the orientation direction of NW to SE has total lateral distance of 241 m with depth ranges up to 11.5 m. The un-interpreted in lines profiles represents the subsurface image (Fig 12 & 14) and the corresponding interpreted inline profiles show sweetness attributes and cavities (Fig 13 & 15). Red circles in Fig 13 represents cavities, showing high contrast impedance which provides low frequency and higher envelope amplitude (Hart 2008). The unsaturated fractures along with cavities have also been displayed in black lines (Fig 15). The first small black line is at a distance of 8 m and depth from 1.5-5.5 m, the second small black line at 20 m distance and 2-5 m depth, and the third large black line at 35 m distance and at 1.5-8 m depth. Similarly, white boxes show saturated fractures and red circles at various locations represent cavities (Fig 15).

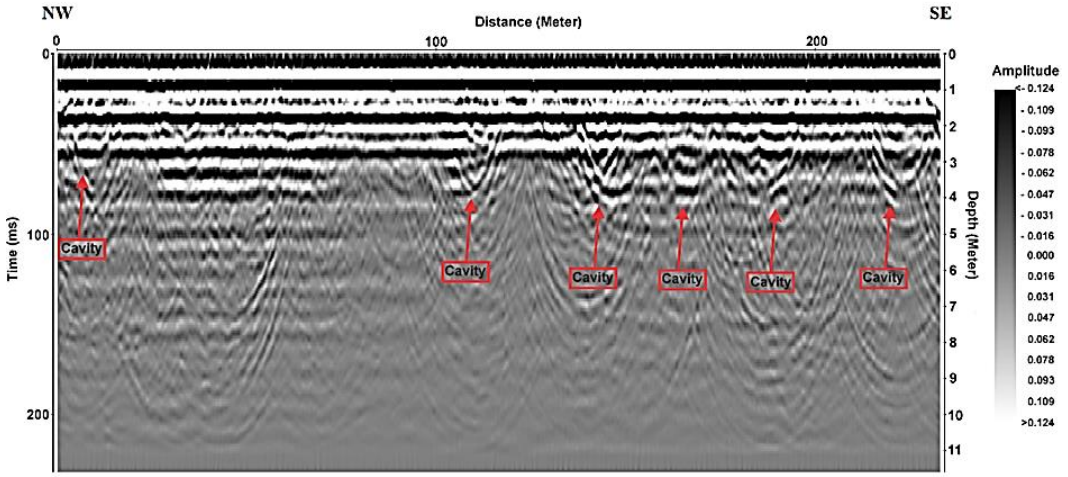

Fig 10. Radargram of Profile-3 detection of cavities at different locations

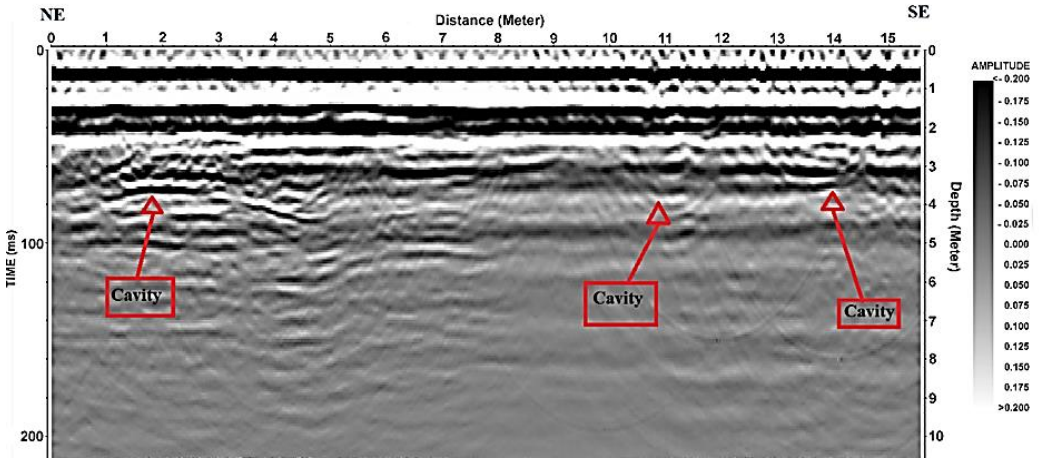

Fig 11. Radargram of Profile-4 detection of cavities at different locations

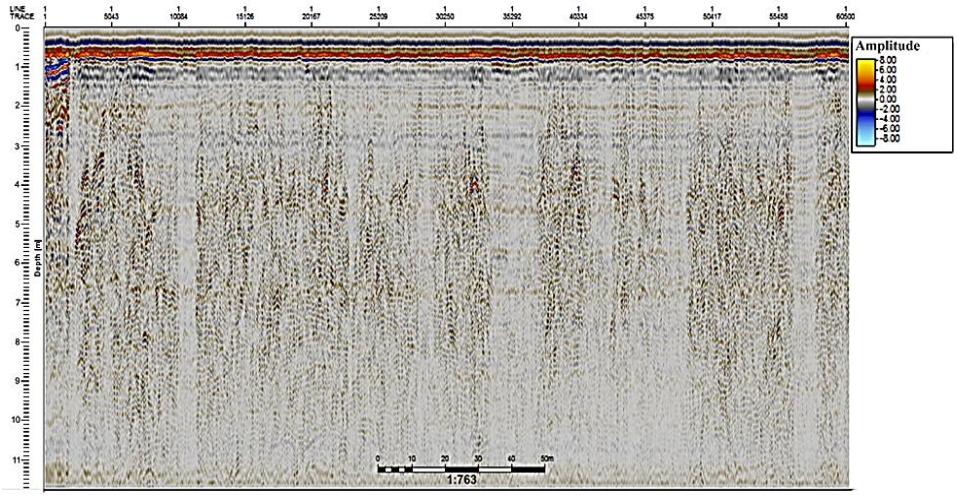

Fig 12. Un-interpreted cross-section of GPR profile-1.

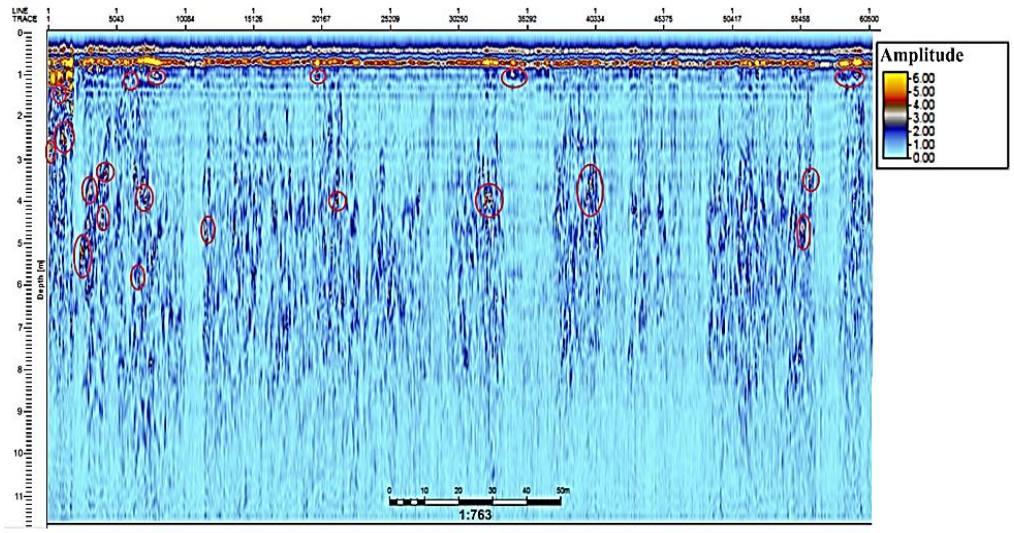

Fig 13. Sweetness attribute of GPR profile 1. Red color circles indicate main cavities

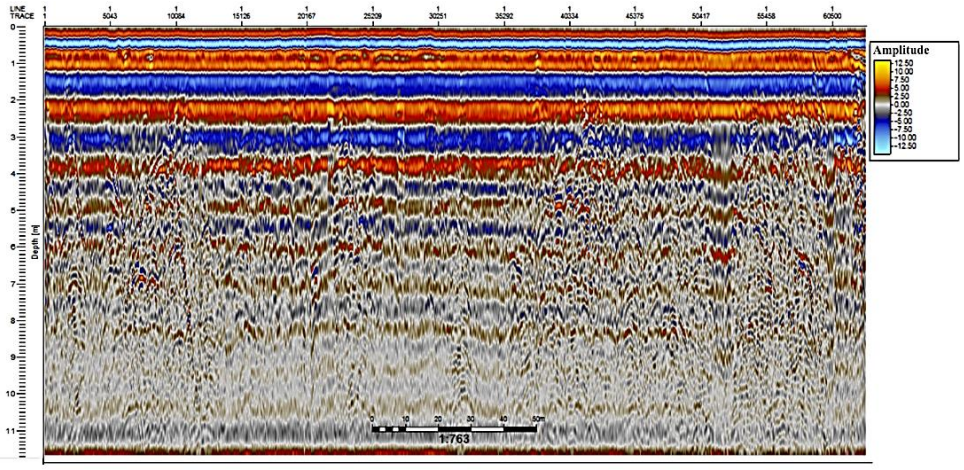

Fig 14. Un-interpreted cross-section of GPR profile-2.

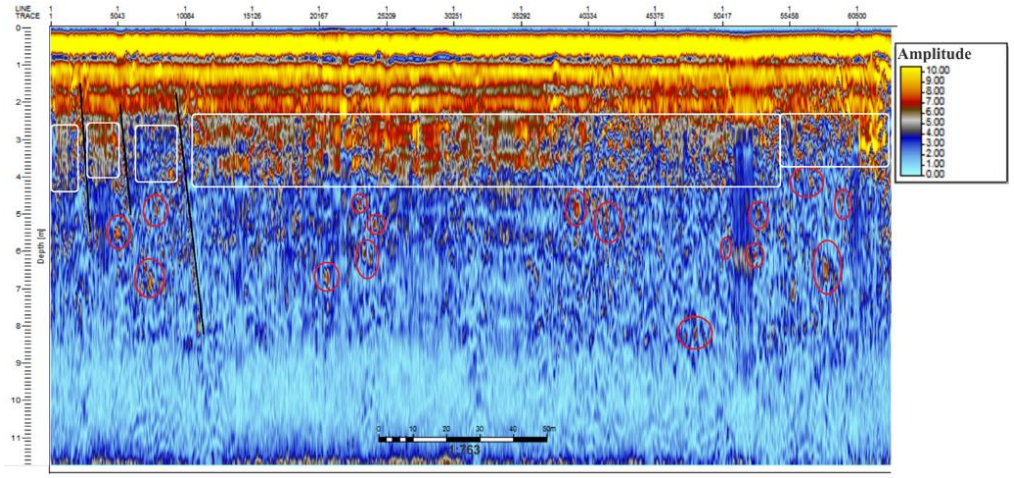

Fig 15. Sweetness attribute of Profile-2. Different colors indicates various cavities (Red color circles= main cavities, black lines= unsaturated fractures and white boxes =Saturated Fractures)

The near surface investigation has been made through MASW data in terms of 2D shear velocity profiles. Shear wave velocity represents Vs30 (upper 30 m layer). Near surface material elastic properties are very important in environmental earth science studies, civil engineering and earthquake geotechnical engineering (Moreno 2015; Rehman et al. 2018). For example, local site conditions are characterized by using Vs30 values for seismic hazard calculations of dam safety which is accepted for the site classification (Dobry et al. 2000; NEHRP Building Seismic Safety Council 2001; IBC 2006). Based on Vs30, all the MASW lines represent that the site lithology has type B (rock) as per NEHRP code (Fig 16). It means that the outcrop is a rocky mass having Vs greater than 760 m/s. It has been observed in all MASW lines that velocity increases with depth, and no low-velocity layer has been detected in the investigation site. From 0 to 50 m depth, the lithology is the same for all profiles (Fig 16).

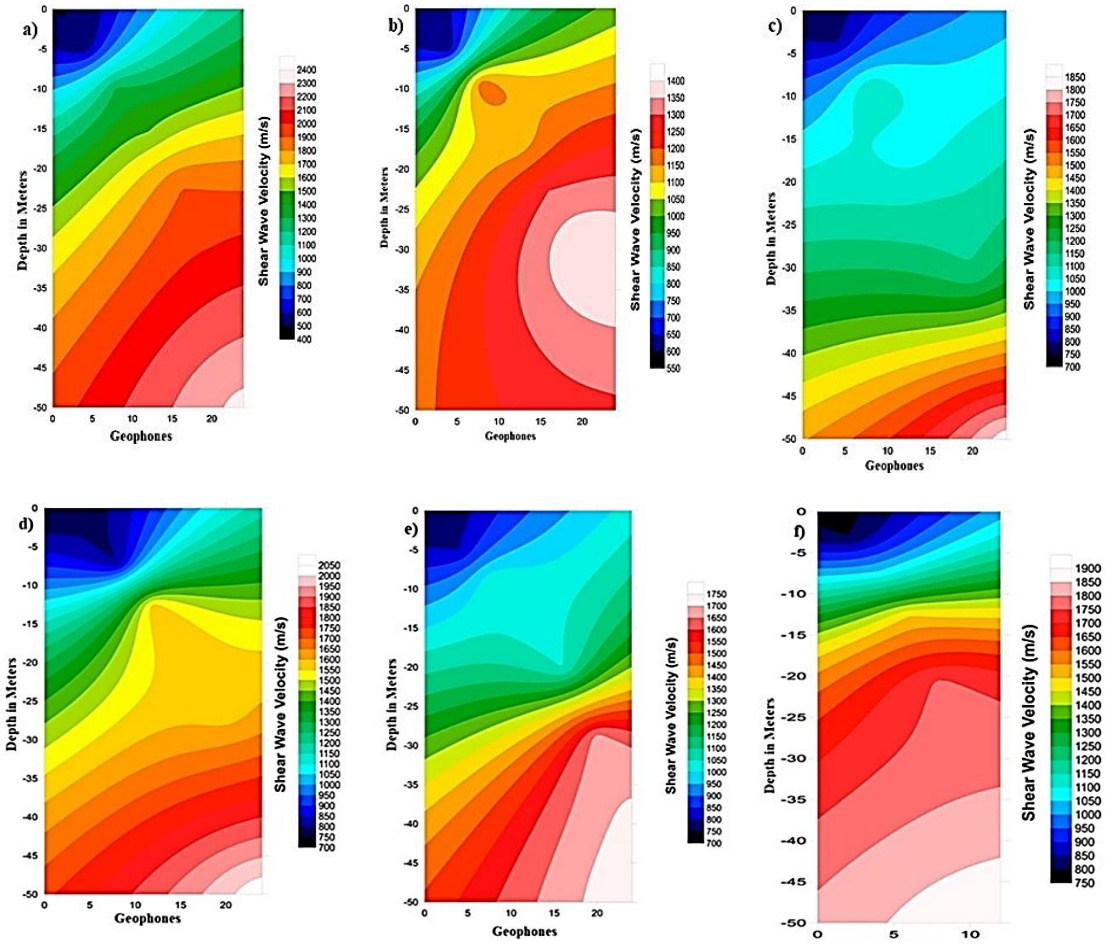

Fig 16. 2-D Profile plots of Geode a: line 1, b: line 2, c: line 3, d: line 4, e: line 5 and f. line 6, all the lines show that as depth increases the Vs also increases

Electrical resistivity tomography (ERT) has been conducted in the study area for investigation of subsurface cavities in terms of 2D pseudosections (Fig 17 & 18). RMS error minimized by performing several processing steps on resistivity profiles and finals results have been prepared for discussion and interpretation after inversion. In ERT Profile-1 (Fig 17), the current was not penetrated through some electrodes due to their installations in bed rock, as a result the data of these electrodes has not been collected up to 32 m distance. Two air-filled Cavities identified having a high resistivity value of more than 46500 Ω-m. The first cavity is found at a distance range of 41-47 m while its diameter has been 6 m and its depth ranges from 2.69 to 5 m. Similarly, the diameter, depth range, and distance range of the second cavity observed are 10 m, 2.69-7 m, and 60-70 m respectively (El-Qady et al. 2005). At a distance of 48 m, a slate bed has been detected having low resistivity values i.e. < 290 Ω-m (Fig 18). The inverted depth of the ERT profile-2 has been prepared upto 16.9 m (Fig 18). In this case, slate bed also depicts low resistivity values i.e. <800 Ω-m and air-filled cavities at a depth of 2-5 m have high resistivity values (>70,000 Ω-m). Several sediment-filled cavities documented at a depth of 2-3.5 m that have also been identified in profile-2 have resistivity values in the range of 2000-5000 Ω-m.

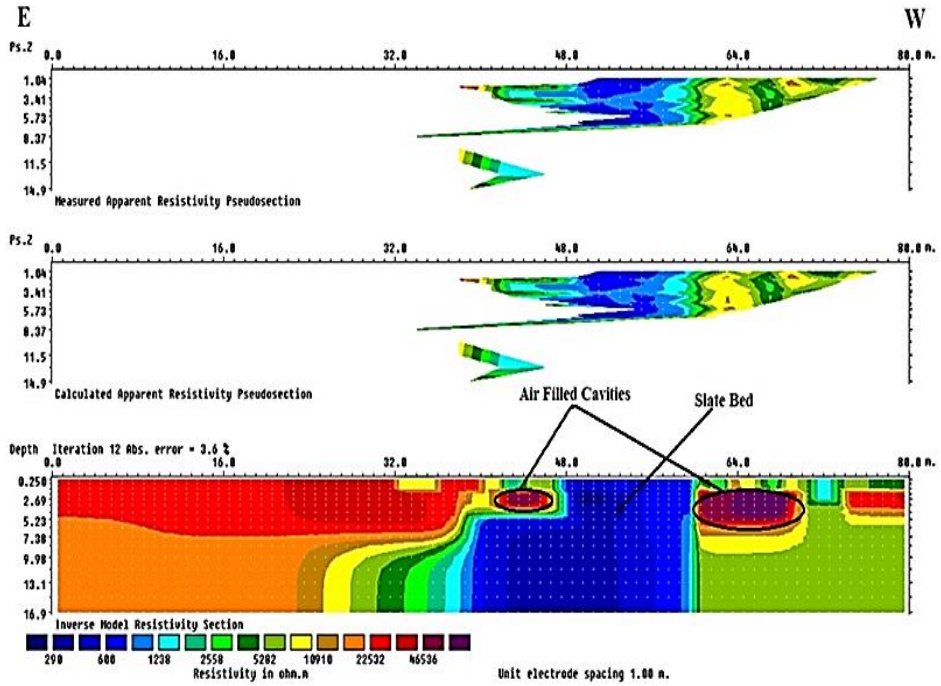

Fig 17. ERT profile-1 showing the measured, calculated and inverted resistivity sections, air filled cavities represented in black circles. Up to 32 m distance the data not collected because of poor electrode connection to ground.

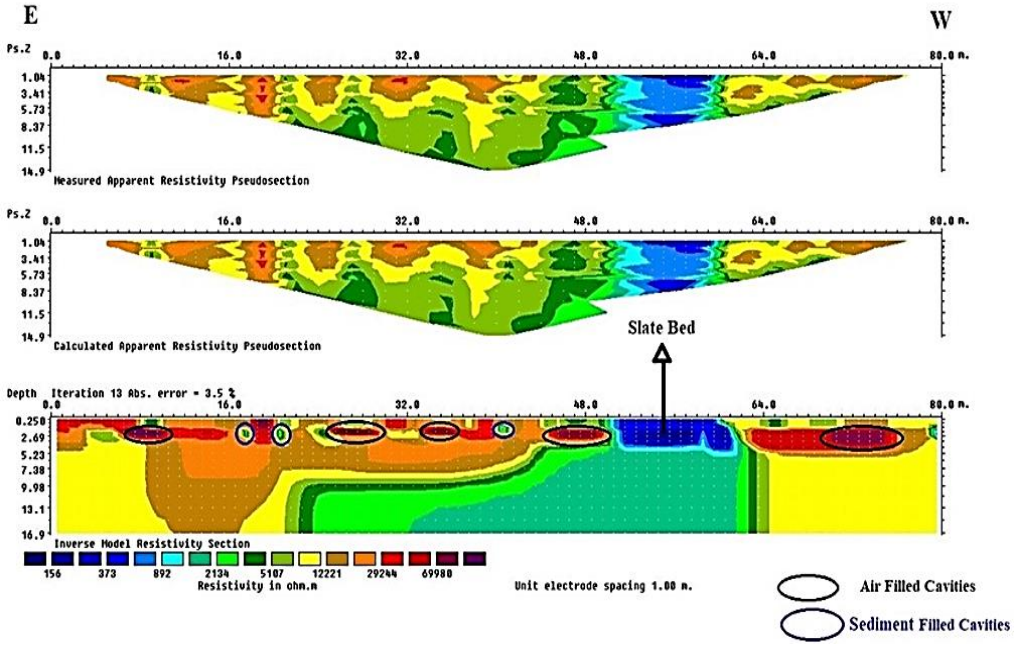

Fig 18. ERT profile-2 having air-filled cavities shown in black circles and sediment filled cavities shown in blue Circle.

In this case, the integrated studies of these three geophysical techniques i.e. GPR, MASW and ERT represent cavities in the same locations. The examples of such cavities are: 1) After integrating the results GPR profile 3 (Fig 10), MASW line 4 (Fig 16) and ERT profile 1 (Fig 17) there was one cavity identified in GPR profile 3 and ERT profile 1. The cavity was identified at 192 meters (m) in GPR profile 3 and 41 m in ERT profile 1 pseudosection having a similar depth of 2-5 m. and 2). At the same distance, there is also a cavity observed on the surface that is shown in Fig 19. We tried to compare the integrated results at some other locations; however, cavities were detected using only GPR. The identification of cavities in the same locations mentioned above using

resistivity and MASW were missing due to its limitations. Furthermore, resistivity results reveals cavities at other locations (Figs. 17 and 18).

To elaborate these results, we included geological information to demonstrate the identified cavities along the profiles. The Gadwalian area limestone has been decomposed through time and formed solution caves / solution channels (Tahirkheli 1971). Most of air-filled and sediment-filled cavities that have been detected through ERT and GPR techniques lie at a depth of 2-7 m at several locations in the study area. Cavities identified through these geophysical techniques represents karstification process and with the passage of time; cavities size and numbers will increase due to water infiltration and dissolution (Veress 2020). There is also a potential threat of subsidence of the strata and collapses in this area.

Fig 19. Cavity observed on the surface at the study area near GPR profile 3 and ERT profile 1.

In this study, GPR has been primarily utilized for cavities detection while ERT and MASW have been used for subsurface imaging. This study infers that GPR and ERT are valuable tools for detecting near-surface cavities. Their results demonstrate the effectiveness of different geophysical methods that can be used for cavities detection in diverse environmental conditions and geological settings. All these geophysical methods have some limitation which depends on the geology and topography of the study area. These limitations may also include architectural barriers i.e. buildings, walls, firm ground (asphalted, paved or bed rocks). In these cases, GPR can play effective role in exploration. In the present research work, some limitations of these three geophysical techniques related to cavities detection and acquisition have also been observed. In 2-D profile plots of MASW and GPR, the depth is not the same because in GPR if the depth increases up to 50 meters the resolution will become low and cavities will not be easily detected. Similarly for small cavities detection through ERT technique, it is required that electrodes should be 1 m apart. According to Reynolds (2011), GPR and ERT technique are primarily used for subsurface cavities detection while seismic refraction technique can also be helpful. The seismic refraction technique in this case has been primarily used for marking subsurface geological contacts, extracting physical properties and subsurface imaging.

5. Conclusion

Dam failures caused a significant amount of property losses and causalities. Through integrated geophysical approach, the Gadwalian dam site has been investigated for safety purposes. The preliminary results obtained are as follow:

•In GPR radargram, several shallow cavities have been identified up to a 12-meter depth at different locations. The sweetness attribute applied to GPR data has been useful and depict several cavities and fractures that are saturated and unsaturated.

•The ERT results represent air and sediment-filled cavities at shallow depth ranging from 2-5 m in the resistivity pseudosections.

•Vs30-based MASW method shows that the study area has competent lithologies in subsurface estimated by higher shear velocities with respect to depth. MASW method has been effectively used for engineering purposes by marking contacts, extracting physical properties and subsurface imaging in this case.

•The integrated geophysical data interpretation validates the existence of subsurface features. The presence of cavities and fractures in the study area represents karstification process is active. If mitigation measures are not taken and this process further increases, it will be hazardous to the dam reservoir. Cement grout filling, concrete filling, engineering fill with geosynthetic materials as reinforcement and compacted engineering fill methods can be used for treatment of these features.

Acknowledgements

The authors are thankful to Dr. Amir Ali, Mr. Wajid Ali, Dr. Sajjad Ahmad and Mr. Waqar Azeem for critical reviews and helpful comments on the manuscript. We are thankful to NCE in Geology, University of Peshawar, Pakistan for providing the research facilities and support. We are also thankful to anonymous reviewers for their useful comments and appreciations.

References

Alastruey I, Alastruey J, Ayuso N, Cuchí J, Lera F, Mediano A, Molina P, Villarroel J, Viñals V, Carrasco F, Durán JJ (2002) Inducciónmagnética y técnicasasociadas en el estudiodel karst. In: Carrasco F, Durán JJ, Andreo B (eds) *Karst and Environment* 505-510.

Alemaw B, Keaitse E, Chaoka T (2016) Management of water supply reservoirs underuncertainties in arid and urbanized environments, *Journal of Water Resource and Protection* 8(11): 990-1009.

Andrus RD, Stokoe II KH (2000) Liquefaction resistance of soils from shear-wave velocity, *Journal of Geotechnical and Geo-Environmental Engineering* 126:1015-1025.

Azeem MW, Rehman K, Rehman NU, Farooq U, Arshad A. (2021) Delineation of sinkhole in evaporite deposits using electrical resistivity survey: a case study of southern Kohat Plateau, Pakistan, *Arabian Journal of Geosciences* 14(4):1-9.

Bessason B, Erlingsson S (2011) Shear wave velocity in surface sediments, *Jökull* 61: 51-64.

Butler DK, Llopis JL (1990) Assessment of anomalous seepage conditions, Geotechnical environment geophysics 2:153-173.

Cedergren HR (1997) Seepage, drainage, and flow nets. John Wiley & Sons, United States.

Chamberlain AT, Sellers W, Proctor C, Coard R (2000) Cave detection in limestone using ground penetrating radar, *Journal of Archaeological Science* 27(10):957-964.

Chinedu AD, Ogah AJ (2013) Electrical resistivity imaging of suspected seepage channels in an earthen dam in Zaria, North-Western Nigeria, *Open Journal of Applied Sciences* 3(1):145-154.

Cook JC (1965) Seismic mapping of underground cavities using reflection amplitudes, *Geophysic*s 30(4):527-538.

Dobry R, Borcherdt RD, Crouse CB, Idriss IM, Joyner WB, Martin GR, Power MS, Rinne EE, Seed RB (2000) New site coefficients and site classification system used in recent building seismic code provisions, *Earthquake Spectra* 16(1):41-67.

Duffy BG (2008) Development of Multichannel Analysis of Surface Waves (MASW) for Characterising the Internal Structure of Active Fault Zones as a Predictive Method of Identifying the Distribution of Ground Deformation. MSc. Thesis, University of Canterbury, Christchurch, New Zealand.

El-Qady G, Hafez M, Abdalla MA, Ushijima K (2005) Imaging subsurface cavities using geoelectric tomography and ground-penetrating radar, *Journal of Cave and Karst Studies* 67(3):174-181.

Farooq M, Park S, Song YS, Kim JH, Tariq M, Abrallam AA (2012) Subsurface cavity detection in a karst environment using electrical resistivity (er): a case study from yongweol-ri, South Korea *Earth Sciences Research Journal* 16(1):75-82.

Flohrer C, Pöpel M (1996) In Combination of a covermeter with a GPR-system: A tool for detecting prestressed bars in concrete structures, Proceedings of the Sixth International Conference on Ground Penetrating Radar. 273-277.

Gambetta M, Armadillo E, Carmisciano C Stefanelli P, Cocchi L, Tontini FC (2011) Determining geophysical properties of a near surface cave through integrated microgravity vertical gradient and electrical resistivity tomography measurements, *Journal of Cave and Karst Studies* 73(1):11-15.

Gibson, P, Lyle P, George D (2004) Application of resistivity and magnetometry geophysical techniques for near-surface investigations in karstic terranes in Ireland, *Journal of Cave and Karst Studies* 66(2):35-38.

Hart BS (2008) Channel detection in 3-D seismic data using sweetness, *AAPG Bulletin* 92(6):733-742.

Hylland MD, Riaz M, Ahmad S (1988) Stratigraphy and structure of the southern Gandghar range, Pakistan, Geol Bull Univ Peshawar 21:1-14.

Hylland MD (1990) Geology of the Southern Gangadhar Range and Kherimar Hills, Northern Pakistan. MS Thesis, Oregon State University, Corvallis, Oregon, USA.

IBC I (2006) International building code. International Code Council, Inc. (formerly BOCA, ICBO and SBCCI) 4051:60478-65795.

Ilesanmi OM, Oladapo A, Olanike O, Steve AF, Oluseun B, William I (2013) Seismic refraction study of Gurara dam phase II, northwestern Nigeria, *Journal of Geology and Mining Research* 5(11):239-249.

Ismail A, Anderson N (2007) Near-surface characterization of a geotechnical site in north east Missouri using shear-wave velocity measurements, *Near Surface Geophysics* 5(5):331-336.

Jehangir Khan M, Ghazi S, Mehmood M, Yazdi A, Naseem AA, Serwar U, Zaheer A, Ullah H (2021) Sedimentological and provenance analysis of the Cretaceous Moro formation Rakhi Gorge, Eastern Sulaiman Range, Pakistan, *Iranian Journal of Earth Sciences* 13 (4), 252-266.

Loke MH (2012) Tutorial: 2-D and 3-D electrical imaging surveys. GeotomoSoftware, Malaysia.

Loke MH (2015) Tutorial: 2-D and 3-D Electrical Imaging Surveys. GeotomoSoftware, Malaysia.

Łyskowski M, Mazurek E, ZITĘK J (2014) Ground Penetrating Radar Investigation of Limestone Karst at the Odstrzelona Cave in Kowala, ŚWIĘTOKRZYSKIE Mountains, Poland, *Journal of Cave and Karst Studies* 76(3):184-190.

Mochales T, Casas A, Pueyo E, Román M, Pocoví A, Soriano M, Ansón D (2008) Detection of underground cavities by combining gravity, magnetic and ground penetrating radar surveys: a case study from the Zaragoza area, NE Spain, *Environmental Geology* 53(5):1067-1077.

Moreno FJM (2015) Detection and characterization of karstic caves: integration of geological and geophysical techniques. PhD dissertation, Universidad de Granada, Granada, Spain.

NEHRP Building Seismic Safety Council (2001) National Earthquake Hazards, Reduction Program (NEHRP) Recommended Provisions for Seismic Regulations for New Buildings and Other Structures. Part 1–Provisions and Part 2–Commentary, Reports No. FEMA-368 and FEMA-369, prepared by the Building Seismic Safety Council for the Federal Emergency Management Agency.

Nouioua I, Boukelloul ML, Fehdi C, Baali F (2013) Detecting sinkholes using ground penetrating radar in DrâaDouamis, Cherea Algeria: A case study, *Electronic Journal of Geotechnical Engineering* 18:1337-1349.

Park CB, Miller RD, Xia J (1999) Multichannel analysis of surface waves, *Geophysics* 64(3):800-808.

Rehman K, Burton P, Weatherill G (2018) Application of Gumbel I and Monte Carlo Methods to assess seismic hazard in and around Pakistan, *Journal of Seismology* 22(3):575-588.

Reynolds JM (2011) An introduction to applied and environmental geophysics. John Wiley & Sons, USA

Robinson ES, Çoruh C (1988) Basic Exploration Geophysics. John Wiley, USA.

Rybakov M, Rotstein Y, Shirman B, Al-Zoubi A (2005) Cave detection near the Dead Sea-a micromagnetic feasibility study, *The Leading Edge* 24(6):585-590.

Riaz M, Hylland MD, Ahmad S, Ghauri A (1991) Structure and stratigraphy of the northern Gandghar range, Hazara, Pakistan, *Journal of Himalayan Earth Sciences* 24:71-84.

Seed H, Duncan J (1981) The Teton dam failure–a retrospective review. Soil mechanics and foundation engineering: proceedings of the 10th international conference on soil mechanics and foundation engineering, Stockholm. pp 15-19.

Sjödahl P, Dahlin T, Johansson S (2009) Embankment dam seepage evaluation from resistivity monitoring data, *Near Surface Geophysics* 7(5-6):463-474.

Smith DL (1986) Application of the pole-dipole resistivity technique to the detection of solution cavities beneath highways, *Geophysics* 51(3):833-837.

Steeples DW, Miller RD (1987) Direct detection of shallow subsurface voids using high-resolution seismic-reflection techniques. In: Multidisciplinary conference on sinkholes and the environmental impacts of karst 2. pp 179-183.

Tahirkheli R (1971) The geology of the Gandghar Range, Distt. Hazara, NWFP, *Geol Bull Univ Peshawar* 6:33-42.

Thierry P, Debeblia N, Bitri A (2005) Geophysical and geological characterisation of karst hazards in urban environments: application to Orléans (France), *Bulletin of EngineeringGeology and the Environment* 64(2):139-150.

Veress M (2020) Karst types and their karstification, *Journal of Earth Science* 31(3):621-634

Wadia DN (1957) Geology of India. Mcmillan and Co, London.

Wills CJ, Petersen M, Bryant WA, Reichle M, Saucedo GJ, Tan S, Taylor G, Treiman J, (2000) A site-conditions map for California based on geology and shear-wave velocity, *Bulletin of the Seismological Society of America 90(6B*): S187-S208.

Xia J, Miller RD, Park CB (1999) Estimation of near-surface shear-wave velocity by inversion of Rayleigh waves, *Geophysics* 64(3):691-700.

Xu X, Zeng Q, Li D, Wu J, Wu X, Shen J (2010) GPR detection of several common subsurface voids inside dikes and dams, *Engineering Geology* 111(1-4):31-42.

Yeats RS, Hussain A (1987) Timing of structural events in the Himalayan foothills ofnorthwestern Pakistan, *Geological society of America bulletin* 99(2):161-176.